EGTRIB Journal
JOURNAL OF
THE EGYPTIAN SOCIETY OF TRIBOLOGY
VOLUME 12, NO. 2, April 2015, pp. 44 - 54 **ISSN 2090 - 5882**

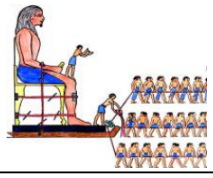

SAND EROSION BEHAVIOUR OF TRANSPARENT PVC THIN FILM COATINGS

Mahmoud M. M.

Production Engineering and Mechanical Design Department, Faculty of Engineering, Minia University, P.O. 61111 El-Minia, Egypt.

ABSTRACT
Sand erosion cause severe damage of headlights, paints and many surface components of the vehicles. In this study, sand erosion testing of the headlight protections was investigated. A test rig was designed and manufactured for sand erosion testing purpose. Four types of transparent polyvinyl chloride commercial coating film materials were tested with two different thicknesses namely, 0.25 and 0.5 mm were tested. Wear was determined at different attack angles by inspecting of the worn surfaces using an optical microscope and by weighting the test specimen before and after sand attack. The opacity of the sand blasted specimens was measured using a resistor photocell. Two wear mechanisms were displayed with regard to the observed results. The first was the pits, holes and scratches due to sand impingement, while the second was sand embedment in the tested surfaces causing a weight gain. The relative opacity of the headlight protections was depended on the sand embedment in the coating and the wear scars which cause the light diffraction.

KEYWORDS
Erosion, sand particles, polyvinyl chloride transparent coatings, thickness, angle of inclination.

INTRODUCTION
Headlight covers are designed to protect the head and tail light lamps of vehicles from damage in both civilian and combat environments. With time, the automobile industry began to take note of the protective benefits of headlight cover film from eroding in the harsh, sandy environments. In Middle East atmosphere, all types of vehicles are subjected to sever sand erosion conditions, because of the high ambient dust concentrations experienced throughout the wide desert areas which accelerate the damage of vehicles body, windows and headlamps due to sand erosion. Particles of the same composition and of differing size upon contact/separation will have a tendency to electrify positively for larger particulates and to electrify negatively for smaller ones, [1 - 3]. It was approved for sand sized quartz particulates, [4] and also of fine quartz (few-micron sized) dust, [5]. This net separation of electric charges (polarities) would then be expected to generate an electric field, specifically consisting of a negatively electrified dust cloud above a positively electrified sand layer. This has been experimentally supported by electric field measurements of terrestrial dust devils. Here electric fields of 30 - 170 kV/m have been seen, [6]. An electric field of this strength was sufficient to

significantly affect the transport of sand and dust in many ways, [7]. Similarly other forms of granular transport can produce electrification and electric fields, this can be problematic in industrial applications. It was noticed that the sand erosion rates of hard ceramics such as tungsten carbide, silicon nitride, silicon carbide, and partially stabilized zirconia have been tested in air-sand erosion facilities, [8]. High-speed photography was used to determine the sand velocity distribution at each test setting. Selection of materials capable of withstanding sand erosion as one of the major problems encountered when designing valves for oil and gas severe service applications, [9 - 11]. The relatively high fluid velocity accelerates entrained sand particles that subsequently impinge onto walls of the valve parts as well as the downstream pipe wall. Testing the erosion resistance of materials at conditions corresponding to those in the field as well as studying the erosion damage mechanism were carried out for both comparing existing materials and understanding the route to better compositions. The angle dependence of the erosion rate was obtained by testing the materials at an impact angle of 30º with the sand velocity of 105 m/s. Brittle materials such as hard ceramics a maximum erosion rate occurs at 90º [12, 13], whereas for ductile materials this occurs at oblique impact angles, [14]. It was found that erosion components, including pure erosion and corrosion-enhanced erosion, are the dominant contributors, while the contribution of corrosion components is slight. With the increase of the sand concentration and slurry flow velocity, the E–C rate of the steel increases. However, an increasing impact angle would decrease the E–C rate of the steel in oil sands slurry. When the potential of the steel is relatively negative, erosion is dominant, especially at high flow velocities. At positive potentials, corrosion of steel is important in E–C process, especially at low flow velocities. Erosion–corrosion (E–C) can generate material loss much greater than the sum of the pure erosion and the pure corrosion individually due to the interaction between them, [15 - 17]. The extent of E–C is dependent on a wide range of variables, [15, 18, 19], including the solid sand particles (mass, hardness, density, size, shape, velocity and impact angle), target material (hardness, metallographic structure, strength, ductility and toughness), and the environment (slurry composition, flow velocity and temperature). Extensive studies have been conducted to understand the effects of various variables on E–C of materials, [20 - 22]. Moreover, the erosion rate of steel increases with the flow velocity. The effect of flow velocity on erosion of metal has been well established, [23]. For pure erosion, the increase in erosion rate with velocity was associated with the increase in kinetic energy of the erodent and number of sand impacts per unit time, causing more effective damage on the metal surface.

It was reported that the erosion rate increases with the sand concentration because of the increased opportunity of sand particles impacting the steel surface. It was proposed, [24], that during each impact, plastic deformation takes place at the vicinity of the impact when the yield strength of steel was locally exceeded. Multiple impacts could generate a plastically deformed layer near the eroded surface with the increased yield strength due to strain hardening, reducing the erosion rate. Results of a large number of erosion tests on artificially generated and relatively dense sand–mud mixtures are presented, [25]. Soil sample compositions are varied concerning clay silt and sand silt ratio, and clay mineralogy. The experimental set-up consists of a recirculating small scale rectangular erosion flume with unidirectional flow conditions. The erosion threshold and erosion rate are studied through step by step increasing the flow rate during a test.

A recent experimental approach to accelerated laboratory testing sand erosion in high pressure flow channels of complicated 3D configurations was developed, [26]. The flow

channels were manufactured from organic glass (PMMA) in separate plates that facilitated weight loss measurements in different parts of the channels as well as erosion visualization. Ceramic composites with different content of TiC were produced by hot pressing, [27]. The effect of TiC content on the microstructure and mechanical properties of this composite has been studied. The sand erosion performance of the nozzles made from this composite was examined with an abrasive air-jet. The hardness of the tested ceramic nozzles had an important influence on the erosion rate in abrasive air-jet machining. The nozzle materials with high hardness showed lower erosion rate.

In the present research, the investigation of common erosive wear of polymeric transparent coating materials, which used to protect headlights with paints and many other surface components of vehicles was conducted. The angle of inclination of the test specimens, the thickness of the coating and the opacity are investigated.

EXPERMENTAL WORK

The erosion test was carried out by an air compressor used to compress atmospheric air to a maximum pressure of 0.8 N/mm^2 (8 bar). The air was stored in a pressurized vessel of 25 litre capacity. The compressor refills automatically when the pressure decreases to 7 bar. A sand blaster was used to eject air mixed with sand. There are two different hoses. The first hose was connected to the bottom of the handle and to the compressor, while the second hose was connected to the bottom of the barrel and attaches the underside of a reservoir that contains sand particles. When the trigger of the gun was pressed, the air passes from the pressurized vessel creates a suction pulling the sand particles up the hose from its reservoir and then through a 3 mm diameter nozzle, see Fig. 1a. The average velocity of the air mixed with the sand particles were calculated by applying Bernoulli equation (30 m/s, 108 km/h). The sand blaster gun was fixed to one side of a test chamber, which was a 450 mm height, 500 mm width and 780 mm long. The specimen held by a clamping device fixed on a holder with a rotation and position adjustment mechanism to control the desired angle of inclination Fig. 1b. In this study the distance from the tip of the nozzle to the specimen was fixed to 100 mm. The duration of the sand blast was 20 seconds. The sand was sieved to control the particles up to 2 mm.

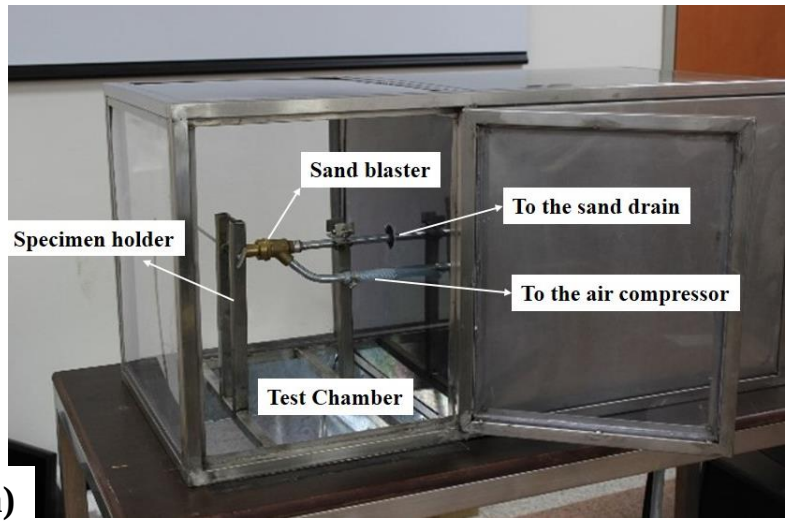

(a)

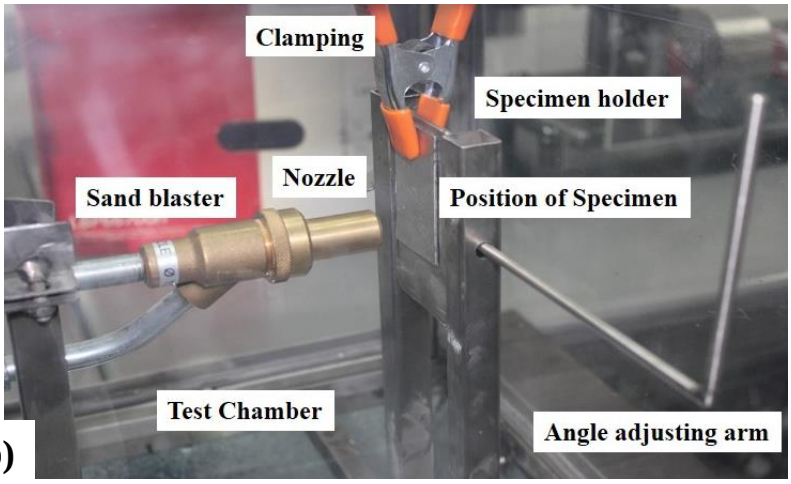

(b)

Fig. 1. Erosion Test Machine

The specimen substrate was made of polymethylmethacrylate (PMMA) which are used in the manufacturing of vehicles light covers sheets of 100 × 100 mm and 5 mm thickness. Four types of transparent polyvinyl chloride commercial coating films were tested (A, B, C, and D). Test specimens were blasted at 20°, 40°, 60°, and 90° inclination angles.
Two thicknesses of the tested sheets 0.25 and 0.5 mm that will be referred in the text as T_1 and T_2 respectively, were tested. The change in the opacity of the tested coatings were measured by a resistor photocell. When light strikes the cell, it allows current to flow more freely. When dark, its resistance increases dramatically. The test rig, used in the present work, was designed and manufactured to measure the opacity by shedding light through the tested sample from the photo resistor that was connected using ohmmeter to measure the resulting resistance, Figs. 2, 3. The opacity was determined by the ratio between the resistance before and after wear.

Fig. 2 Photograph of the photocell.

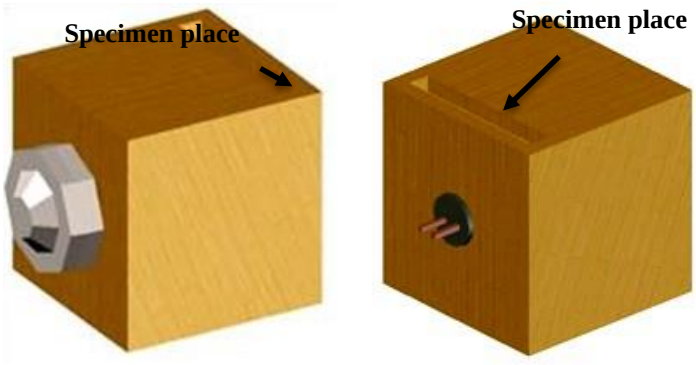

Front view **Rear view**

Fig. 3 Test rig used to measure opacity.

RESULTS AND DISCUSSION

The photomicrographs of the surfaces of coating (A) after sand blast were shown in Fig. 4. It was clearly shown that at 20º angle of inclination, relatively big sand particles were embedded in the coating surface. As the angle if inclination increased ability of sand particles to embed decreased. Besides, as the coating thickness increased to (T2), the number of embedded sand particles increased. The evidence of the embedment of sand particles into the coating surface (B) is shown in Fig. 5. The big sand particles were embedded at relatively higher inclination angles, 60 and 90º. The severity of embedment was not influenced by the thickness of the coating. The ability of the coatings to be embedded by relatively small sand particles increased at 40º angle of inclination. Coatings (C) suffered more damage at 20º angle of inclination for the two tested thickness, Fig. 6. As the angle of inclination increased, embedment decreased. It seems that this coating type had relatively low shear strength. Photomicrographs of coating (D) after sand blast showed the severest damage particularly for the lower thickness, Fig. 7. The plastic deformation caused by the abrasion of sand particles was more pronounced for that coating for all angle of inclination. Based on that observation it was recommended to avoid use of the coating (D) in application in abrasive media.

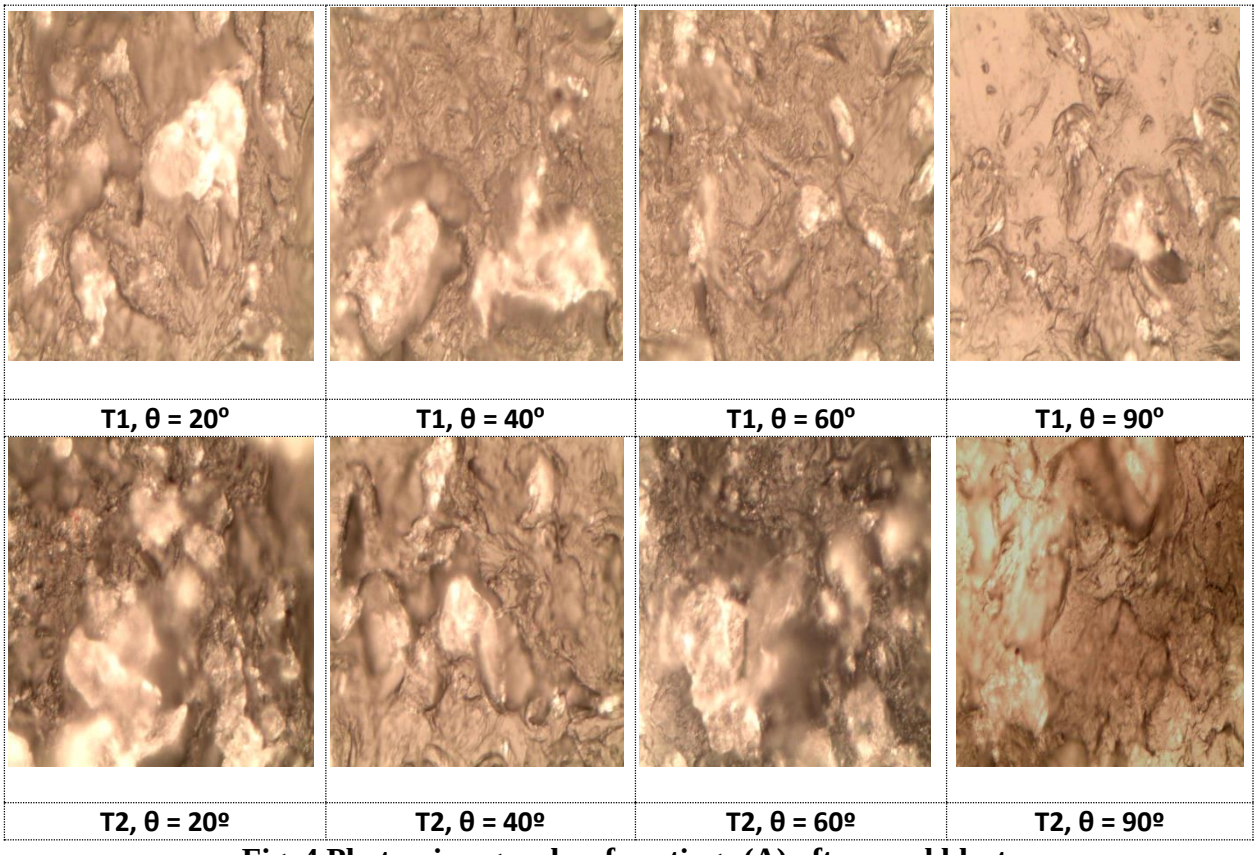

Fig. 4 Photomicrographs of coatings (A) after sand blast.

T1, θ = 20º	T1, θ = 40º	T1, θ = 60º	T1, θ = 90º
T2, θ = 20º	T2, θ = 40º	T2, θ = 60º	T2, θ = 90º

Fig. 5 Photomicrographs of coatings (B) after sand blast.

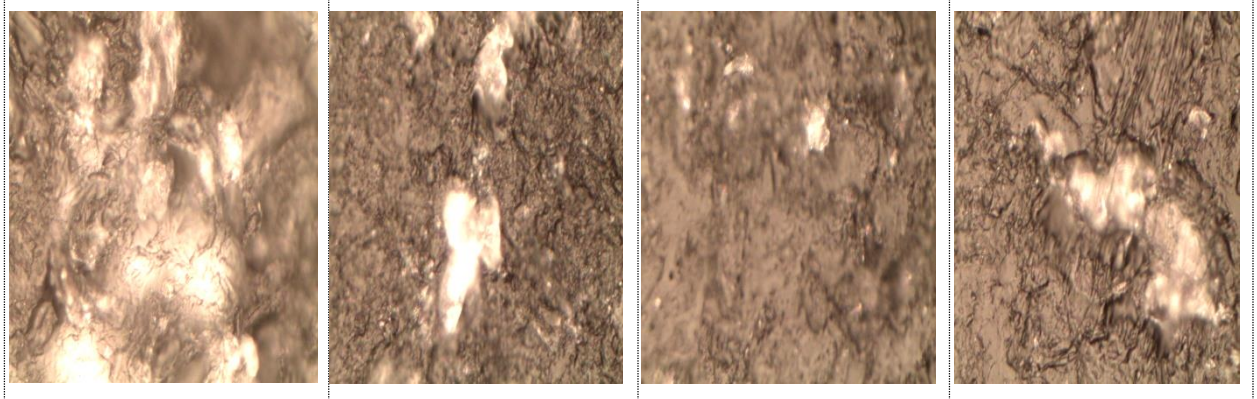

T1, θ = 20º	T1, θ = 40º	T1, θ = 60º	T1, θ = 90º
T2, θ = 20º	T2, θ = 40º	T2, θ = 60º	T2, θ = 90º

Fig. 6 Photomicrographs of coatings (C) after sand blast.

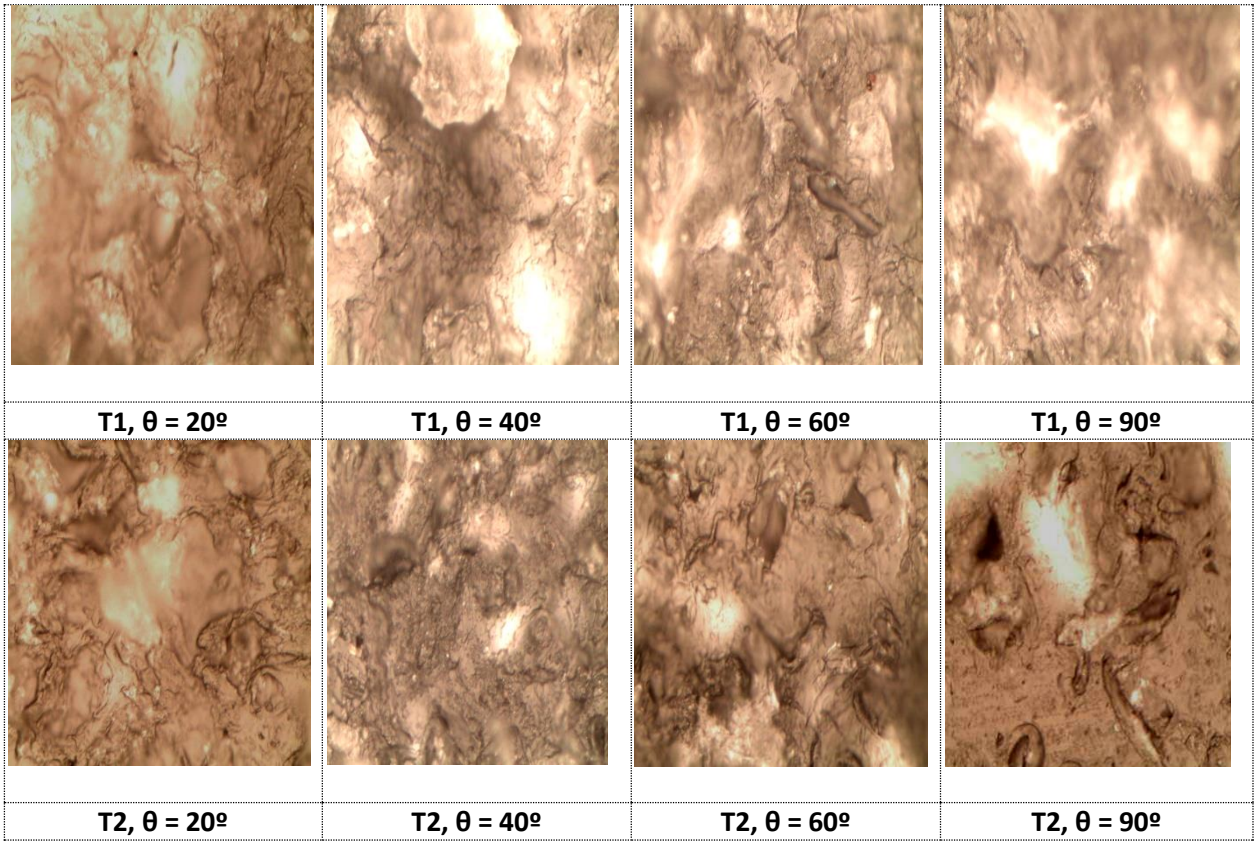

Fig. 7 Photomicrographs of coatings (D) after sand blast.

The results of the experiments carried out to investigate the wear as well as the opacity of the tested transparent coating are illustrated in Figs. 8 – 15. For layer of lower thickness (T1) of the tested coating (A), wear showed lower values than that displayed by T2. Wear significantly increased with increasing angle of inclination, Fig. 8. It was known that opacity depends on the sand particles embedment in the coating (A) as well the wear marks occurred by particle impact which increased light diffraction. A significant increase in the relative opacity was observed for coating (A) of T1 thickness, where the highest opacity was observed at 90° angle of inclination. As the angle of inclination increased opacity increased, Fig. 9. The opacity increased as result of the sand particles embedment in the film coating or as the damage caused by the plastic deformation of the surface increased.

Wear of transparent PVC coatings (B) showed a decreasing trend with increasing angle of inclination, Fig. 10. The embedment of sand particles in the polymer surface reflected by the weight increase of the tested coaings after test was quite severe. This observation can be confirmed by the evidence of the embedment of sand particles into the coating surface (B), Fig. 5, where the big sand particles were embedded at 60 and 90º inclination angles. A significant increase in relative opacity was observed for higher coating thickness (T2), Fig. 11. As the angle of inclination increased opacity increased. It was known that opacity depends on the sand particles embedment in the coating (B) as well as the wear marks and plastic deformation occurred by particle impact which increased light diffraction.

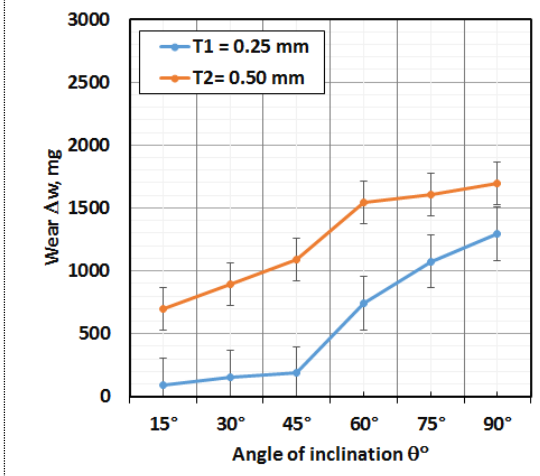

Fig. 8 Wear of transparent PVC coatings (A).

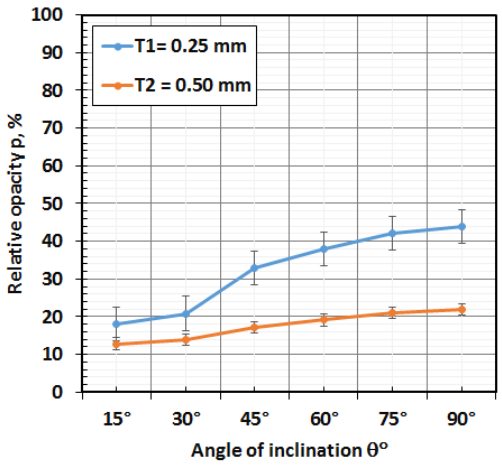

Fig. 9 Relative opacity of transparent PVC coatings (A).

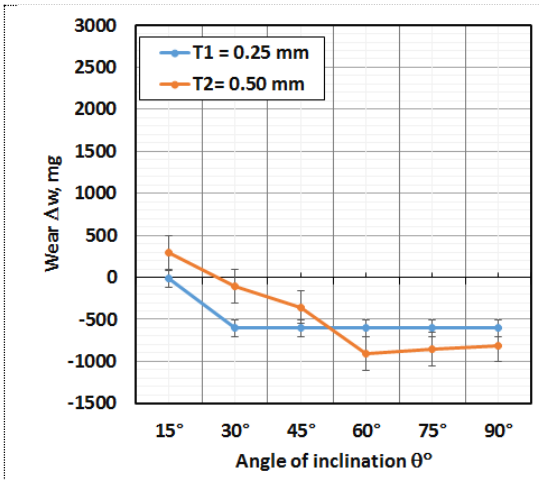

Fig. 10 Wear of transparent PVC coatings (B).

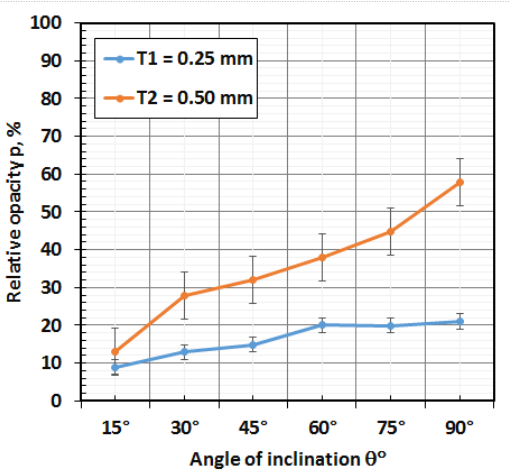

Fig. 11 Relative opacity of transparent PVC coatings (B).

For the single layer of the tested coating (C), wear showed the highest value at 20° and 40° angle of inclination. As the film thickness increased wear increased. Embedment of sand particles in the polymer surface significantly increased with increasing angle of inclination, Fig. 12. The coating of relatively higher thickness showed the highest embedment. Besides, a significant increase in relative opacity was observed for higher coating thickness (T2), Fig. 13, where the highest opacity was observed at 20° angle of inclination. As the angle of inclination increased opacity increased.

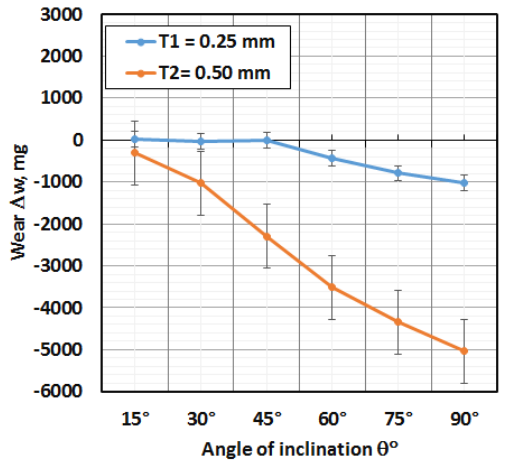

Fig. 12 Wear of transparent PVC coatings (C).

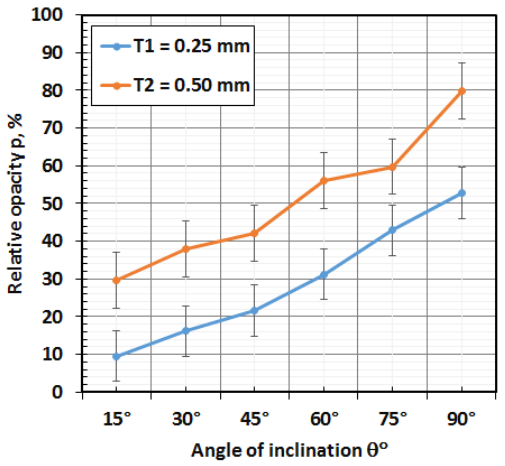

Fig. 13 Relative opacity of transparent PVC coatings (C).

For the single layer of the tested coating (D), wear showed the highest value at 20° angle of inclination. As the coating thickness increased wear increased. Embedment significantly increased with increasing angle of inclination, Fig. 14. The severity of embedment of coatings (D) was lower than that observed for coating (B) and (C). A significant increase in relative opacity was observed for the lower coating thickness (T1), where the highest opacity was observed at 90° angle of inclination, Fig. 15. The opacity increased as result of the sand particles embedment in the film coating, and that was confirmed by the photomicrographs of coatings (D) after sand blast, Fig. 7. The coating of (T2) thickness showed relatively low opacity.

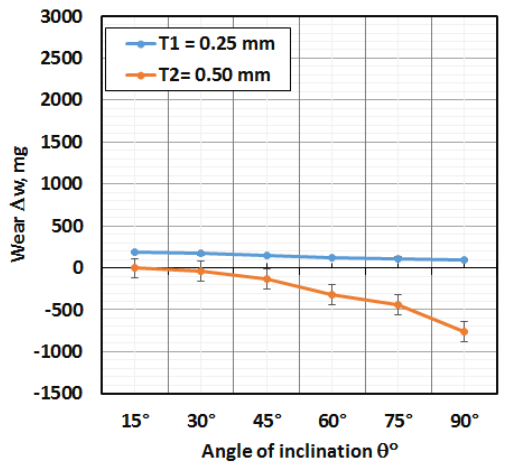

Fig. 14 Wear of transparent PVC coatings (D).

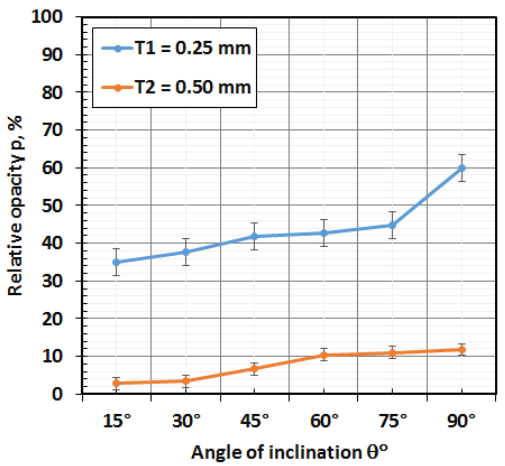

Fig. 15 Relative opacity of transparent PVC coatings (D).

CONCLUSIONS

1. It was clearly shown that at 20° angle of inclination, relatively big sand particles were embedded in the coating surface. As the angle of inclination increased ability of sand particles to embed decreased. Besides, as the coating thickness increased, the number of embedded sand particles increased.

2. As the film thickness increased wear increased. Wear significantly increased with increasing angle of inclination. It was known that opacity depends on the sand particles embedment in the coating as well the wear marks occurred by particle impact which increased light diffraction. As the angle of inclination increased opacity increased. The opacity increased as a result of the sand particles embedment in the film coating or as the damage caused by the plastic deformation of the surface increased

3. Wear of transparent PVC coatings showed a decreasing trend with increasing angle of inclination. The embedment of sand particles in the polymer surface reflected by the weight increase of the tested coaings after test was quite severe. This observation can be confirmed by the evidence of the embedment of sand particles into the coating surface, where the big sand particles were embedded at 60° and 90º inclination angles.

4. The severity of embedment of coatings differs from one to another.

REFERENCES

1. Lacks, J. D., Duff, N., Kumar, S. K., "Nonequilibrium accumulation of surface species and triboelectric charging in single component particulate systems", Phys. Rev. Lett. 100, 188305, (2008). DOI: 10.1103/PhysRevLett.100.188305.

2. Kok, J. F., Lacks, D. J., "Electrification of granular systems of identical insulators", Phys. Rev. E79, 051304, (2009). DOI: 10.1103/PhysRevE.79.051304.

3. Lacks, D. J., Levandovsky, A., "Effect of particle size distribution on the polarity of triboelectric charging in granular insulator systems ", J. Electrostat. 65, pp. 107 - 112, (2007). DOI: 10.1016/j.elstat.2006.07.010

4.Forward, K. M., Lacks, D. J., Sankaran, R. M., "Charge segregation depends on particle size in triboelectrically charged granular materials ", Phys. Rev. Lett. 102, 028001, (2009). DOI: 10.1103/PhysRevLett.102.028001.

5. Merrison, J. P., Gunnlaugsson, H. P., Hogg, M. R., Jensen, M., Lykke, J. M., Bo Madsen, M., Nielsen, M. B., Nonberg, P., Ottosen, T. A., Pedersen, R. T., Pedersen, S., Sorensen,A. V., "Factors affecting the electrification of wind-driven dust studied with laboratory simulations", Planetary and Space Science, 60 (1), pp. 328–335 (2011). DOI:10.1016/j.pss.2011.10.008.

6. Jackson T. L., Farrell W. M., "Electrostatic fields in dust devils: An analog to mars", IEEE Transactions on Geoscience and remote sensing. 44 (10), pp. 2942 - 2949, (2002). DOI: 10.1109/TGRS.2006.875785.

7. Lorenz, R. D., Shandera, S. E., "Target effects during penetrator emplacement: heating, triboelectric charging, and mechanical disruption", Planet. Space Sci. 50, pp. 163 - 179, (2006). DOI: 10.1016/S0032-0633(01)00108-8.

8. Celotta D. W., Qureshi U. A., Stepanov E. V., Goulet D. P., Hunter J., Buckberry C. H., Hill R., Sherikar S. V., Moshrefi-Torbati M., Wood R. J. K., "Sand erosion testing of novel compositions of hard ceramics", Wear 263 , pp. 278 - 283, (2007). DOI: 10.1016/j.wear.2007.01.098.

9. Wheeler D. W., Wood R. J. K., "Erosion of hard surface coatings for use in offshore gate valves", Wear 258, pp. 526 – 536, (2005). DOI: 10.1016/j.wear.2004.03.035.

10. Wheeler D. W., Wood R. J. K., "Solid particle erosion of diamond coatings under non-normal impact angles", Wear 250, 795 – 801, (2001). DOI: 10.1016/S0043-1648(01)00733-5.

11. Allen C., Sheen M., Williams J., Pugsley V. A., "The wear of ultrafine WC - Co hard metals", Wear 250, pp. 604 – 610, (2001). DOI: 10.1016/S0043-1648(01)00667-6.

12. Sapate S. G., Rama Rao A. V., "Effect of erodent particle hardness on velocity exponent in erosion of steels and cast irons", Mater. Manuf. Processes 18, pp. 783 – 802, (2003). DOI: 10.1081/AMP-120024975.

13. Bose K., Wood R. J. K., "High velocity solid particle erosion behavior of CVD boron carbide on tungsten carbide", Wear 258, pp. 366 – 376, (2005). DOI: 10.1016/j.wear.2004.06.005.
14. Yang Y., Cheng Y. F., "Parametric effects on the erosion–corrosion rate and mechanism of carbon steel pipes in oil sands slurry" , Wear 276– 277 , pp. 141- 148, (2012). DOI: 10.1016/j.wear.2011.12.010
15. Stack M. M., Pungwiwat N., "Particulate erosion–corrosion of Al in aqueous conditions: some perspectives on pH effects on the erosion–corrosion map", Tribol. Int. 35, pp. 651 – 660, (2002). DOI: 10.1016/S0301-679X (02)00056-7.
16. Neville A., Reyes M., Xu H., "Examining corrosion effects and corrosion/erosion interactions on metallic materials in aqueous slurries", Tribol. Int. 35, pp. 643 - 652, (2002). DOI: 10.1016/S0301-679X (02)00055-5.
17. Rajahram S. S., Harvey T. J., Wood R. J. K., "Erosion–Corrosion resistance of engineering materials in various test conditions", Wear 267, pp. 244 - 254, (2009). DOI: 10.1016/j.wear.2009.01.052.
18. Burstein G. T., Sasaki K. K., "Effect of impact angle on slurry erosion–corrosion of 304 L stainless steel", Wear 240, pp. 80 – 94, (2000). DOI: 10.1016/S0043-1648(00)00344-6.
19. Jana B. D., Stack M. M., "Modeling impact angle effects on erosion–corrosion of pure metals: construction of materials performance maps", Wear 259, pp. 243 - 255, (2005). DOI: 10.1016/j.wear.2005.02.012.
20. Abbade N. P., Crnkovic S. J., "Sand-water slurry erosion of API 5L X65 pipe steels quenched from intercritical temperature", Tribol. Int. 33, pp. 811- 816, (2000). DOI: 10.1016/S0301-679X (00)00126-2.
21. Meng H., Hu X., Neville A., "A systematic erosion–corrosion study of two stainless steels in marine conditions via experimental design", Wear 263, pp. 355 - 362, (2007). DOI: 10.1016/j.wear.2006.12.007.
22. Zhang G. A., Xu L. Y., Cheng Y. F., "Investigation of erosion–corrosion of 3003 aluminum alloy in ethylene glycol–water solution by impingement jet system", Corros. Sci. 51, pp. 283 - 290, (2009). DOI: 10.1016/j.corsci.2008.10.026.
23. Tang X., Xu L. Y., Cheng Y. F., "Electrochemical corrosion behavior of X-65 steel in the simulated oil sand slurry. II: synergism of erosion and corrosion", Corros. Sci. 50, pp. 1469 - 1474, (2008). DOI: 10.1016/j.corsci.2008.01.019.
24. Barik R. C., Wharton J. A., Wood R. J. K., Stokes K. R., "Electro-mechanical interactions during erosion–corrosion", Wear 267, pp. 1900 - 1908, (2009). DOI: 10.1016/j.wear.2009.03.011.
25. Atkinson M. M., Stepanov E. V., Goulet D. P., Sherikar S. V., Hunter J., "High pressure testing sand erosion in 3D flow channels and correlation with CFD", Wear 263 , pp. 270 - 277, (2007). DOI: 10.1016/j.wear.2007.01.100.
26. Jianxin D., Junlong S., "Sand erosion performance of B4C based ceramic nozzles", International Journal of Refractory Metals & Hard Materials 26, pp. 128 - 134, (2008). DOI: 10.1016/j.ijrmhm.2007.06.001.
27. Guanghong Z., Hongyan D., Yue Z., Nianlian L., "Corrosion–Erosion Wear behaviors of 13Cr24Mn0.44N stainless steel in saline–sand slurry", Tribology International 43 , pp. 891 - 896 , (2010). DOI: 10.1016/j.triboint.2009.12.021.